polymer papers

Dynamic structure and aqueous accessibility of poly(*p*-phenylene terephthalamide) crystallites*

C. L. Jackson†, R. J. Schadt†, K. H. Gardner, D. B. Chase, S. R. Allen, V. Gabara and A. D. English‡

DuPont Central Research and Development and DuPont Fibers, Experimental Station, Wilmington, DE 19880–0356, USA

(Received 19 April 1993; revised 15 September 1993)

A more complete description of the morphology of poly(*p*-phenylene terephthalamide) (PPTA) in both as-polymerized polymer and various fibre forms is developed by the utilization of a number of methods (dark-field transmission electron microscopy, X-ray diffraction, solid state n.m.r. spectroscopy, and partial isotopic exchange of accessible amide moieties). This description focuses primarily on the effect of lateral crystallite dimensions on the microscopic dynamic structure and the concomitant macroscopic accessibility properties. The observation of a heterogeneous dynamic structure reflects the imperfect structural consolidation during the processing of PPTA in both as-polymerized polymer and fibre forms. The imperfect microcrystalline structure formed during processing is shown to be the origin of macroscopic accessibility for small molecules and also provides a plausible structural basis for biological accessibility.

(Keywords: PPTA; dynamic structure; macroscopic accessibility)

INTRODUCTION

Symmetric aromatic polyamides have many remarkable and unique properties due, in part, to their large persistence length[1]. Fibres prepared from one of these polymers, poly(*p*-phenylene terephthalamide) (PPTA), are of commercial interest because of their high tenacity, high modulus and high temperature stability[2,3]. The morphology of as-polymerized polymer, fibres and films is controlled to a large extent by the coagulation conditions employed when the polymer is precipitated from solution[4,5]. The morphology of these materials has been the subject of a very large number of independent investigations utilizing a number of approaches[6] such as X-ray diffraction[7–13], electron microscopy[14–16], i.r. spectroscopy[17,18], Raman spectroscopy[19,20], n.m.r. spectroscopy[21–31], etc. Our approach is to co-ordinate the use of a number of methods [encompassing dark-field transmission electron microscopy (TEM), X-ray diffraction, solid state n.m.r. spectroscopy, and partial isotopic exchange of accessible amide moieties] to build a more complete picture of the morphology of this polymer in a variety of forms.

The microscopic model of the morphology of PPTA may be used as a basis for developing an understanding of structure–property relationships. Of particular interest has been the relationship between the morphology and mechanical properties[32–37]. More recently, the role that the morphology plays in the accessibility of the polymer to small molecules as exemplified by gas transport[38] and water sorption has been of interest[39–41]. In this paper, we relate the microscopic morphological model both to the microscopic dynamic structure and to the macroscopic accessibility to water. This correlation gives some insight into the role that the morphology plays not only in the accessibility of PPTA to small molecules, but also the biological degradability of these fibres.

EXPERIMENTAL

X-ray diffraction measurements

Fibre samples were prepared for X-ray diffraction experiments by wrapping commercial yarns onto a flat steel frame (~1 mm thick) to make a single yarn thick parallel array. The two sides of the wrap were pressed together to remove the gap between them. As-polymerized PPTA powder was compressed (KBr press) into a thin film and placed between sheets of 1 μm Mylar® film.

X-ray diffractometry scans from the as-polymerized PPTA sample were collected in the symmetrical transmission mode using an automated Philips diffractometer (curved crystal monochromator, 1° divergence and receiving slits, sample rotating, CuKα radiation, $\lambda = 0.15406$ nm). Data were collected in a fixed time mode with a step size of 0.05° and run from 4 to 60° 2θ. The background scattering in each diffraction scan was fit with a cubic spline and removed. [It was found that equivalent data were obtained when the diffraction scan was truncated to the region of interest (5–40° 2θ) and a straight line, fit to the first and last point of the data,

* Contribution no. 6539

† Present address: NIST, Polymer Division, Building 224, Gaithersburg, MD 20899, USA

‡ To whom correspondence should be addressed

0032-3861/94/06/1123–09

used to define the background.] Reflection positions and widths were best fit by deconvoluting the pattern into broad Gaussian peaks corresponding to the 110, 200 and 211 reflections and an instrumental broadening correction of 0.20° was applied.

Equatorial X-ray diffractometry scans from the Kevlar® yarns were collected in the symmetrical transmission mode using a Huber 4-circle diffractometer equipped with a Braun linear position sensitive detector on the X7a beamline at the National Synchrotron Light Source ($\lambda = 0.070014$ nm). Data were collected over the angular range of 4–35° 2θ with an approximate step size of 0.007°. The background was removed from the region of interest (5–15° 2θ) by subtracting a smooth background from each raw diffractogram using a straight line defined by points with 2θ values of 5 and 15°. Reflection positions and widths were best fit by deconvoluting the pattern into Lorentzian peaks corresponding to the 110, 200 and 211 reflections. The 211 reflection was observed in all samples except for the Kevlar® 149 yarn. No instrumental broadening correction was applied. The crystallite size (persistence length, L) for the 110 and 200 reflections for all samples was determined using the Scherrer equation $[L = (0.89\lambda)/(\beta \cos\theta)]$.

Specimen preparation, TEM and image analysis

Longitudinal fibre sections were prepared by thin-sectioning of fibres mounted in EPOFIX® resin using a DuPont–Sorvall ultramicrotome with a 35° diamond knife. Use of a low-angle knife minimizes compression damage to the fibres. Thin sections (nominally 50–80 nm) were mounted on 200-mesh carbon-coated copper grids.

Selected area electron diffraction patterns and dark-field images were obtained with a Jeol 2000 FX microscope operating at 200 keV utilizing low-dose techniques [small condenser aperture (20–40 μm), small spot size, reduced beam current, a beam blanker to preserve specimen integrity, and short camera lengths of 20–30 cm]. The high resolution beam tilting method was used to obtain dark-field images for the 110 and 200 reflections simultaneously. The two reflections could not be imaged separately due to their close proximity in the diffraction pattern.

For each fibre type, the maximum magnification at which a well-focused image could be produced was determined. Ten-fold enlargements of the dark-field images were used to facilitate identification of individual crystallites. Measurements of the sizes of the bright white areas (representing the crystals) were then made using a 10× ocular lens on a light box. Approximately 1000 crystals were measured for Kevlar® 49 and 1800 for Kevlar® 149. Most of the crystals were fairly symmetric, but the longest dimension was recorded in the case of asymmetric shapes. Note that the determination of the crystallite size distribution for an asymmetric crystal is complicated by the simultaneous imaging of the 110 and 200 reflections (see Results).

As-polymerized and amide deuterated polymer preparation

PPTA as-polymerized polymer (inherent viscosity $= 6.2\,\mathrm{dl\,g^{-1}}$, measured as a 0.5 wt% solution in 100% sulfuric acid at 30°C) was prepared by reaction of *p*-phenylene diamine (PPD) with terephthaloyl chloride (TCl) in an 8% solution of $CaCl_2$ in *N*-methylpyrrolidone. In a three-necked resin kettle equipped with a stirrer and dry nitrogen purge, PPD (5.3 g) was dissolved in the solvent system (180 g) and the temperature was lowered to 10°C by external cooling with ice. TCl (10.0 g) was added into the mixture and the agitator speed was increased to maintain mixing as the viscosity of the reaction mixture increased. The material solidified into a gel and then broke into fine particles. After 15 min the reaction was terminated by addition of water. The polymer was washed with water to remove solvent and salt, then the polymer was air dried.

The PPTA as-polymerized polymer was then vacuum dried (100°C) under N_2 to constant weight, dissolved at 1 wt% concentration in 96% D_2SO_4 (99% deuterated; MSD Isotopes) and stirred at room temperature for 1 week under N_2. Then the polymer was precipitated in cold D_2O (99.99% deuterated; MSD Isotopes), filtered, washed with D_2O to neutrality, and vacuum dried (100°C) to constant weight under N_2. Some hydrolytic degradation occurred during this treatment as evidenced by an inherent viscosity of $2.5\,\mathrm{dl\,g^{-1}}$; however, the number-average molecular weight was still appreciable ($\sim 9000\,\mathrm{g\,mol^{-1}}$). Prior to the n.m.r. measurements, the sample was vacuum-dried (230°C) under N_2 for 2 days. A solid state n.m.r. spin count relative to a PPTA sample in which all of the terephthalamide rings were per-deuterated indicated that 95 ± 5% of the N-H sites were converted to N-D as a result of the procedure given here.

N.m.r. measurements

Fully relaxed ^2H n.m.r. spectra and associated spin-lattice relaxation data were obtained at 20°C intervals over a calibrated temperature range of −184 to 228°C with a Bruker MSL 200 spectrometer operating at a resonance frequency of 30.72 MHz using a previously described procedure[31,42]. Spin-lattice relaxation times (T_1) were measured using a saturation recovery method[31,42]. Spin-lattice relaxation of the selectively deuterated amide sites (N-D) was non-exponential and could be decomposed in the time domain into two components whose relaxation times differed by at least a factor of 18 over the temperature range of −184 to 228°C. Values of T_1, calculated from the evolution of the total magnetization in the time domain, were determined by least squares fitting of the data to a sum of two exponentials corresponding to a fast-relaxing component ($T_{1\mathrm{short}}$) and a slow-relaxing component ($T_{1\mathrm{long}}$). Fully relaxed spectra were acquired with a quadrupolar echo pulse sequence[31,42], using a 2.8 μs $\pi/2$ radiofrequency pulse length and delay times (τ_1) between quadrature pulses of 20, 40, 80, and 160 μs, with the recycle delay time adjusted so that it was at least five times the spin-lattice relaxation time of the slowest relaxing component ($T_{1\mathrm{long}}$) in the spectrum at a given temperature.

N.m.r. lineshape calculation

Using a simplified model for the dynamics of the N-D bonds in N-deuterated PPTA polymer (see Results), lineshapes were calculated for discrete, equal population, two site jumps coupled with an inhomogeneous distribution [$P(\Delta\theta)$] of rapid small-angle fluctuations (rapid librational motion)[42] using a previously described multisite exchange program running on a Cray YMP or Silicon Graphics-R-4D/280SX system[31,42]. This program generates a zero-delay ($\tau_1 = 0$) lineshape which is corrected for echo distortions and convoluted with Gaussian and Lorentzian broadenings, but correction for molecular motion during

the radiofrequency pulses was not attempted[31,42]. All calculations utilized the orientation of the static field gradient tensor, with $|V_3|>|V_2|\geq|V_1|$, determined for collagen[43]. A Gaussian broadening of 2.5 kHz, determined from comparison of calculated lineshapes to the low temperature spectra, was used to account for residual dipolar interactions to both ^2H and ^1H neighbouring nuclei. The Lorentzian broadening corresponds to the value used for processing of the experimental data (1 kHz full width half maximum). Since the $\pi/2$ pulse length of 2.8 μs was previously determined to be lengthened by the non-purely resistive load characteristics of the n.m.r. probe[42], all calculations used the previously utilized 3.2 μs pulse length.

FT-Raman spectroscopy

To determine the extent of N-H to N-D exchange in a variety of experiments, *FT*-Raman spectra were acquired using 300 mW of 1.064 μm radiation from a LDI 3000 diode pumped Nd/YAG laser. Scattered radiation was analysed by a Nicolet 800 series interferometer equipped with a *FT*-Raman accessory. A Ge detector (North Coast, NEP = 10^{-15} W $Hz^{-1/2}$) was used, and Rayleigh line filtering was accomplished with two Kaiser Optical Super Notch® holographic filters. Two thousand scans (2 cm^{-1} nominal resolution) were averaged resulting in a total measurement time of 1 h, and the intensities were corrected for instrument response using a calibrated tungsten source. Spectra obtained after extensive irradiation established that no detectable polymer degradation occurred during collection of the spectra. A slight fluorescent background was observed, but this did not obscure the Raman features of interest.

The extent of N-H to N-D exchange can be followed by measuring the intensities of bands associated with normal modes which have some contribution from N-H motion. The obvious mode to monitor is the N-H stretch at 3350 cm^{-1}. However, at high Raman shifts (corresponding to the N-H stretch region), the noise becomes limiting due to poor detector response. Thus, the best band integrals to determine the extent of deuterium exchange occur in the fingerprint region (1800–700 cm^{-1}). Several bands were integrated in this region: C=O amide I (1674–1632 cm^{-1}), C=C ring (1632–1585 cm^{-1}), amide II (1541–1480 cm^{-1}), NH def. 1 (1360–1298 cm^{-1}), and NH def. 2 (1298–1229 cm^{-1}). For each polymer or fibre sample, all measured intensities were normalized to the C=C ring band integral since the ring mode intensity is minimally affected by deuteration at the amide sites. The resulting intensities for each sample were then referenced to the respective protonated polymer or fibre sample. These spectroscopic results were calibrated relative to an absolute standard provided by a solid state n.m.r. spin count on the PPTA N-D polymer (see Experimental).

Amide H/D exchange

PPTA polymer, Kevlar® 29, Kevlar® 49 and Kevlar® 149 fibres were vacuum dried (100°C) under N_2 to constant weight and then slurried in D_2O for periods of at least 1 day at room temperature under N_2. (The fibres were all cut to 3 cm lengths.) Subsequently, each sample was washed and filtered three times in D_2O (but not to dryness, in order to minimize exposure to atmospheric moisture) using a 60 ml, coarse sintered glass Buchner funnel, and then vacuum dried (100°C) under N_2 to constant weight. Each sample was then packed in 5 mm diameter glass tubes (Kontes Scientific Glassware/Instruments) for *FT*-Raman spectroscopic analysis. The inherent viscosity of PPTA polymer after this procedure was 6.1 dl g^{-1} indicating that no hydrolytic degradation occurred during this process.

RESULTS

Crystallite size

Typical high resolution dark-field TEM images from the 110/200 reflections of Kevlar® 49 and Kevlar® 149 fibres are shown in *Figures 1* and *2*, respectively. Kevlar® 149 had the largest crystals, the Kevlar® 49 crystals were substantially smaller, and the Kevlar® 29 crystallites were too small to be measured by this method. The crystallite size distributions for Kevlar® 49 and Kevlar® 149 were measured as described above and converted to the size-weighted distributions shown in *Figure 3* (by multiplying the frequency with which a given crystallite size was detected by its size) to enable a more direct comparison to the X-ray results. These results illustrate that not only is the *average* crystallite dimension orthogonal to the chain axis direction larger for Kevlar® 149 than for Kevlar® 49 (8.9 nm *versus* 4.7 nm), but that a bimodal distribution of crystallite sizes is observed for Kevlar® 149. This latter observation is not associated with the skin–core structure previously found[44], but rather is associated with the substantial asymmetry of

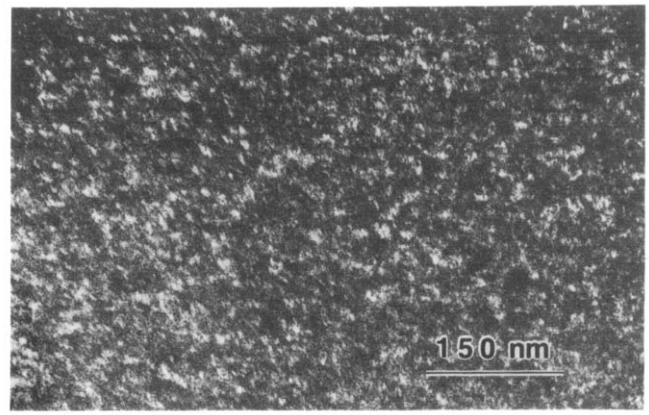

Figure 1 Transmission electron micrograph of Kevlar® 49, dark-field image of 110/200 equatorial reflections. The fibre axis is in the plane of the micrograph

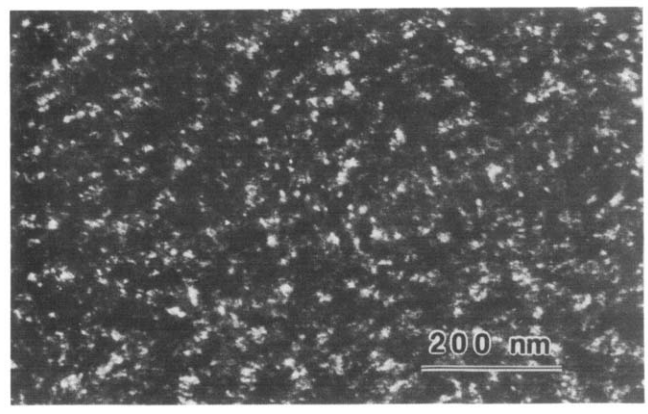

Figure 2 Transmission electron micrograph of Kevlar® 149, dark-field image of 110/200 equatorial reflections. The fibre axis is in the plane of the micrograph

the crystallite cross-section and the fact that the 110 and 200 reflections are being imaged simultaneously. Because it was not possible to separately image the 110 and 200 reflections, it is impossible from these results alone to determine which reflection gives rise to each of the two peaks in the distribution at 13.5 and 7.0 nm; however, comparison to the X-ray results indicates that these are the 110 and 200 reflections, respectively. Note that a potential source of error for the dimensions determined with this method is that a small angular misorientation of the crystal results in failure to meet the Bragg condition due to the short wavelength of the electron; however, as previously shown[4,5], crystals as small as those observed here (3–13 nm) are not seriously affected by this limitation. In any case, the TEM results are in fairly good agreement with the X-ray data as is shown on the abscissa of *Figure 3*.

X-ray diffraction data collected for as-polymerized PPTA polymer showed that both the 110 and 200 peaks were quite broad. The crystallite size calculated from these two reflections (using the Scherrer equation) indicated that the crystallites are approximately circular in cross-section for the plane orthogonal to the chain axis direction with a characteristic dimension of 3–3.5 nm. *Figure 4* illustrates a representation of the crystallite cross-section for PPTA as-polymerized polymer with the unit cell dimensions given for convenience. (Note the large fraction of the chains located on the crystallite surface.)

X-ray diffraction data for the fibre specimens were collected using the synchrotron source to eliminate the need to apply instrumental broadening corrections. *Figure 5* illustrates the diffraction patterns obtained from

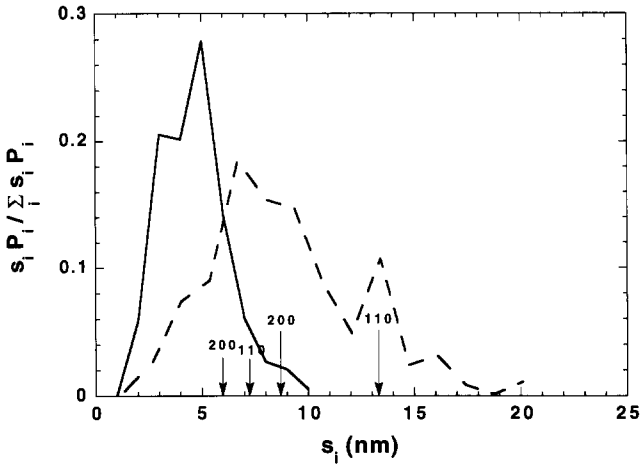

Figure 3 Normalized size weighted distributions ($s_i p_i / \sum s_i p_i$) of crystallite sizes (s_i) for Kevlar® 49 (——) and Kevlar® 149 fibres (– – –). Values for crystallite size determined from X-ray diffraction are indicated on the abscissa with the two arrows on the left-hand side referring to Kevlar® 49 and the two arrows on the right-hand side referring to Kevlar® 149

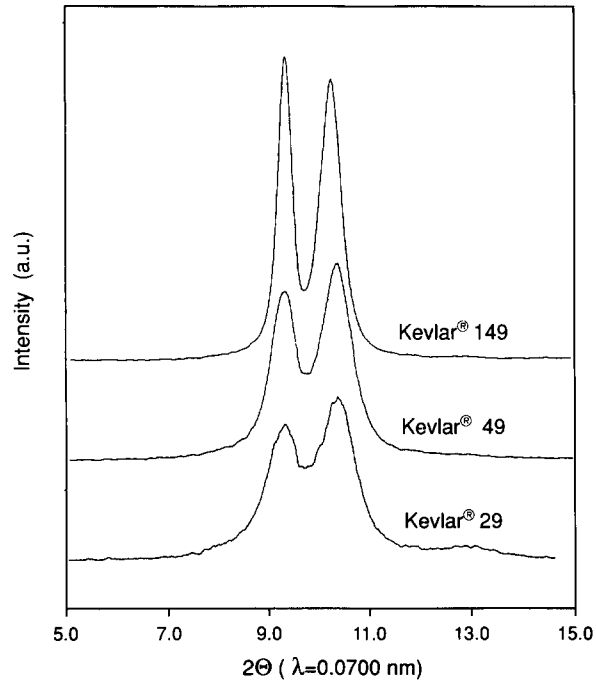

Figure 5 X-ray diffraction patterns at ambient temperature of Kevlar® 29, Kevlar® 49 and Kevlar® 149

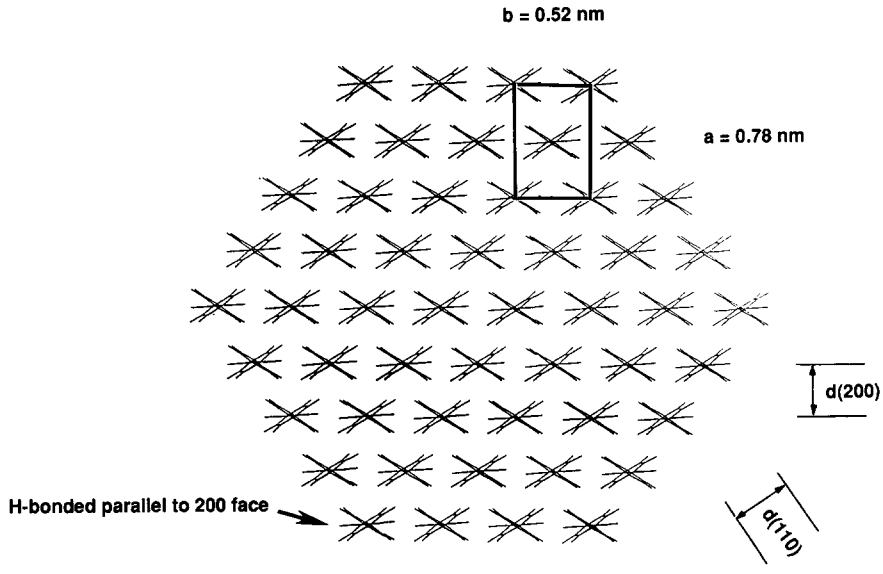

Figure 4 Schematic diagram of the cross-section of an as-polymerized PPTA crystal illustrating the unit cell and the large fraction of molecules residing on the surface of the crystallite; crystal size shown is 3.1 × 3.6 nm

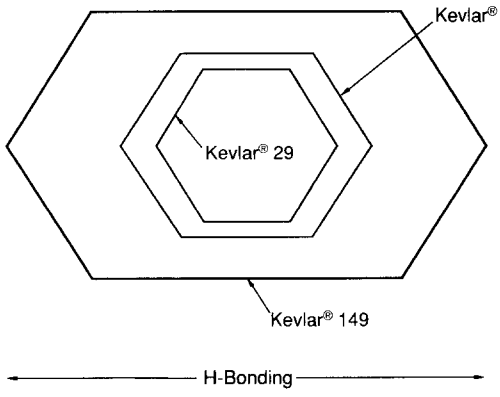

Figure 6 Schematic diagram of crystallites in Kevlar® fibres in cross-section, showing preferential growth along the *b*-direction as the crystallite perfection is increased during fibre processing. Cross-sectional boundaries are defined by the 110 and 200 planes

Table 1 PPTA polymer and Kevlar® fibre mean crystallite sizes (nm)

Form	*h k l*	X-ray	DF/TEM
PPTA as-polymerized	1 1 0	3.5	
polymer	2 0 0	3.5	
Kevlar® 29	1 1 0	5.2 (4.81)[a]	(3.2)[a]
	2 0 0	5.1 (3.95)[a]	
Kevlar® 49	1 1 0	7.2 (6.54)[a] (6.4)[c]	⟨4.7⟩ (4.9)[a]
	2 0 0	6.0 (5.28)[a]	
Kevlar® 149	1 1 0	13.3 (>10)[b] (5–22)[c]	⟨8.9⟩ 13.5[d]
	2 0 0	8.7	7.0[d]

DF, dark field
[a] Reference 15
[b] Reference 46
[c] SAXS from reference 44
[d] Maxima of distribution

equatorial scans for the three fibres (Kevlar® 29, 49 and 149). *Figure 6* schematically illustrates that in the series Kevlar® 29, Kevlar® 49 and Kevlar® 149, the mean crystallite size increases and the crystallites become increasingly asymmetric. The asymmetry reflects preferential crystal growth along the hydrogen-bonded direction (*b*-axis) as the fibre structure is increasingly perfected during processing.

Table 1 gives values of crystallite sizes for all three fibres and as-polymerized polymer from this and previous work. The *average* crystallite dimensions for Kevlar® 49 and 149 fibres obtained from TEM are about three-quarters that derived from X-ray diffraction for both the 110 and 200 reflections. It is expected that the crystallite dimensions found from the TEM results will be reduced to some degree by the effect of small angular misorientation (discussed above) and/or twisting along the long axis of the crystal; the X-ray result will more heavily weight larger crystals since they are more efficiently detected than are smaller crystallites. Given these caveats the *average* crystallite dimensions measured by these two methods are in surprisingly good agreement. For Kevlar® 149 the agreement between the X-ray (13.3 nm, 8.7 nm) and TEM (13.5 nm, 7.0 nm) results for the dimensions associated with the individual reflections (110, 200) is exceptionally good. Lastly, note that the crystallite sizes determined here and previously[15,44,46] are all in fairly good agreement considering the fairly large instrumental broadening correction necessary for the data not acquired with a synchrotron source.

Table 2 illustrates that while the *d*-spacing of Kevlar® 29 and 49 are essentially identical, the different *d*-spacings observed for Kevlar® 149 are thought to be outside of experimental error. These changes indicate that the *a* dimension is slightly larger and the *b* dimension is slightly smaller for Kevlar® 149. These observations indicate that the spacing between the hydrogen-bonded sheets has on average increased slightly and the spacing within the hydrogen-bonded sheet has on average decreased. These dimensional changes could be accounted for either by an increase of the dihedral angle of the phenyl rings with respect to the amide plane or by the fact that the increased crystallite size gives rise to a more perfect average structure which has the observed average *d*-spacings.

Amide bond dynamics via ^2H n.m.r. spectroscopy

The fully relaxed, quadrupolar echo experimental and calculated ^2H n.m.r. lineshapes ($\tau_1 = 40\,\mu s$) for N-deuterated PPTA polymer at −184 and 228°C are shown in *Figure 7* illustrating the maximum variation of the experimental lineshape over this temperature range. Comparison to calculated lineshapes indicates that the experimental lineshape is a composite of two lineshapes assigned, respectively, to two dynamically distinct, *temperature-independent* populations of amide bonds associated with a large fraction (~75%) of essentially rigid N-D bonds and a smaller fraction (~25%) of N-D bonds exhibiting large angle jumps. The geometry of the molecular mechanics model for the amide bond dynamics is based on using the proposed bond angles, derived from X-ray diffraction studies, of the 1,4 axes of the phenylene groups in the diamine and terephthalamide moieties with respect to the amide group; furthermore, the model assumes a bimodal distribution of correlation times for the N-D jumping process, wherein the rigid-like component is assigned a $\tau_c > 10^{-1}$ s and the jumping component a $\tau_c < 10^{-9}$ s. More elaborate correlation time distributions are not justified experimentally. For example, unless the distribution in jumping rates is extremely broad, a significant population in the intermediate exchange regime ($\tau_c = 10^{-5}$–10^{-7} s) would exist leading to a delay time (τ_1) dependence in the quadrupole echo lineshapes[47]. The experimental lineshapes show essentially no delay time dependence in the range from 20 to 160 μs. Additionally, the librational motion (discussed below) must be in the fast motion regime for both components of the lineshape because of the observation, again, of the absence of a delay time dependence of the lineshapes.

To a first approximation, the observed splitting between the outermost singularities of the experimental lineshape is characteristic of essentially rigid amide (N-D) bonds with a quadrupolar coupling constant (e^2qQ/h) of ~210 kHz and $\eta = 0.2$. Generally, quadrupole interaction tensors for deuterium attached to nitrogen exhibit

Table 2 Kevlar® fibre unit cell dimensions (nm)

Fibre	*h k l*	*d* spacing
Kevlar® 29	1 1 0	0.435
	2 0 0	0.389
Kevlar® 49	1 1 0	0.434
	2 0 0	0.390
Kevlar® 149	1 1 0	0.433
	2 0 0	0.394

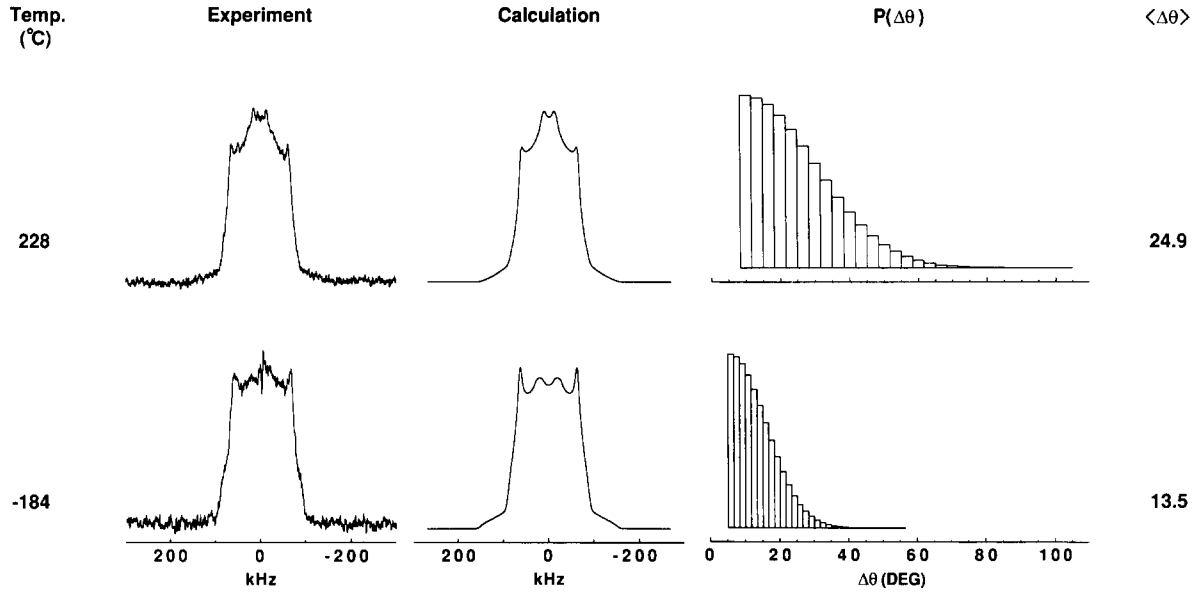

Figure 7 ^{2}H n.m.r. (30.7 MHz) experimental and calculated lineshapes for amide-deuterated PPTA polymer showing the maximal lineshape variation over a temperature range of −184 to 228°C. The librational amplitude distribution $P(\Delta\theta)$ and the mean librational amplitude $\langle\Delta\theta\rangle$ for the calculated lineshapes are also shown

substantial variation in magnitude and asymmetry primarily due to the strong influence of hydrogen bonding[48]. These values for the quadrupole coupling constant and η are quite reasonable when compared to those obtained for N-D bond dynamics in the crystalline phase of nylon 66[42]. From N-D studies of urea[48,49], it is also known that the effect of ^{14}N-D dipolar coupling on the experimental n.m.r. lineshape may introduce an error on the order of 2 kHz for the quadrupole coupling constant and 1–2% error in η.

The splitting of the two innermost lineshape singularities is characteristic of $\sim 180°$ jumps ($e^2qQ/h = 210$ kHz; $\eta = 0.2$) of the N-D bond about the 1,4 axis of the terephthalamide rings, and may not be simulated by jumps or librations of significantly smaller amplitude. In addition, because the frequency position of these lineshape singularities is well defined, any distribution (Gaussian) in jump angles about the large angle (180°) jump must have a standard deviation of $< 10°$. Lineshape calculations revealed that the splitting of the two central peaks in the experimental lineshapes (*Figure 7*) could not be satisfactorily reproduced by selecting the 1,4 axis of the diamine rings as the axis about which the N-D bond jumps. However, a qualitatively better fit to the central portion of the experimental lineshape was achieved by including a variation of 1–2° in the angle between the N-D bond and the 1,4 axis of the terephthalamide rings (molecular dynamics axis).

Furthermore, the addition of rapid librational motion to the nearly rigid component is necessary to best fit the vertical edges of the experimental lineshapes (*Figure 7*). While at high temperatures, it is found that the addition of rapid librational motion to the 180° jumping component is required to match the experimental lineshape intensity between the V_1^* peaks (between the innermost peaks; *Figure 7*). Rapid librational motions are introduced as inhomogeneous Gaussian distributions [$P(\Delta\theta)$] of amplitudes, characterized by a most probable amplitude, a low amplitude cut-off, and a standard deviation, which may differ for the essentially rigid component and large angle jumping component[42]. However, the simulations revealed that for each temperature the same Gaussian distribution of librational amplitudes could be used for both the non-jumping and jumping components to compose a calculated lineshape which corresponds to the experimental lineshape. V_2 is appreciably averaged by the librational motion so that the vertical edges of the lineshape are smeared out by the Gaussian distribution of rapid librations. In contrast, the frequency position of the innermost singularities defined by $V_1^* \sim V_1$ are not significantly affected by the rapid librational motion.

As the temperature is increased, the experimental spectra apparently show an increased contribution from the large angle jumping component as evidenced qualitatively by increases in the intensity of the lineshape between the V_1 singularities (*Figure 7*). However, calculations indicate the experimental lineshape is composed of two essentially *temperature-independent* components associated with a large fraction of amide bonds which are relatively rigid and a minor component ($\sim 25\%$) associated with a large angle jump motion of the N-D bonds. Further calculations reveal that the difference between the low and high temperature experimental spectra results from a variation in the Gaussian distribution of rapid librations where the mean librational amplitude $\langle\Delta\theta\rangle$ (*Figure 7*) nearly doubles in the temperature range from −184 to 228°C. The temperature independent fraction of N-D bonds ($\sim 25\%$) executing large angle jumps may be contrasted with the large variation observed in the fraction of π-flipping terephthalamide rings[30] and diamine rings[31] over the same temperature range.

Additional evidence for the presence of two dynamically differentiated populations of amide groups with the less mobile component comprising $\sim 75\%$ of the sites is available from the ^{2}H n.m.r. spin lattice relaxation data. While the spin lattice relaxation time of the slowest relaxing component in a two-component model varies from 40 to 1.5 s over the temperature range of −184 to 75°C, the fractional population falls in the range of $75 \pm 10\%$ over this entire range; at higher temperatures (228°C) this population is reduced to $\sim 50\%$ evidently

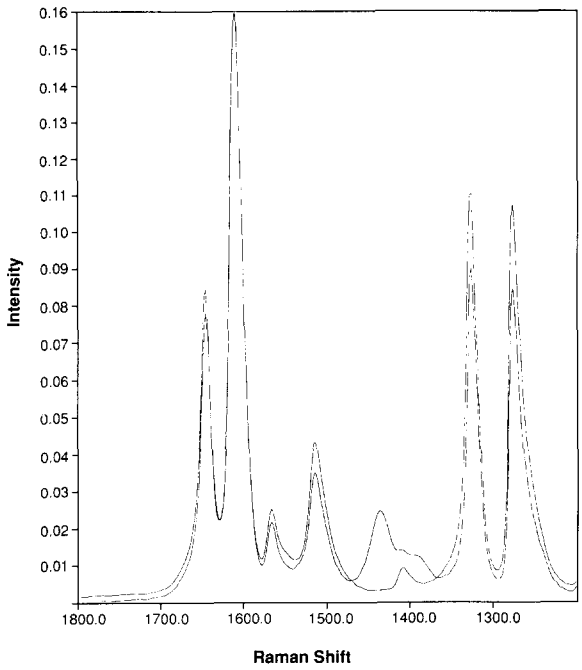

Figure 8 *FT*-Raman spectra for PPTA fibres treated with either H_2O (upper curve in the 1300 cm^{-1} region) or D_2O. Spectra are normalized to C=C band (1632–1585 cm^{-1})

by the presence of considerable motion in nearby terephthalamide[30] and diamine rings[31]. Additionally, the longer spin lattice relaxation time component of the terephthalamide and diamine rings shows a virtually temperature independent population (near 75%) over the same temperature range[31]. Thus it appears that it is the mobile amide sites which give rise to the spin lattice relaxation time differentiation of not only the amide sites, but the terephthalamide and diamine ring sites as well, into two populations of 75% less mobile and 25% more mobile over the temperature range of −184 to 75°C.

Amide accessibility

Amide sites located on the surface of crystallites are expected to be not only more mobile, but also more accessible to small molecules than are sites located at the interior of a crystallite. Based upon this premise we developed a method (see earlier) to evaluate the accessibility of amide sites in PPTA to exchange with water (D_2O). The fraction of amide sites that have been exchanged from N-H to N-D is determined by *FT*-Raman spectroscopy. Utilizing this approach we have determined that for PPTA as-polymerized polymer ~30–40% of the amide sites are exchanged; whereas for chopped fibre we observe ~25% exchange for Kevlar® 29 and Kevlar® 49 and ~10% exchange for Kevlar® 149. *Figure 8* illustrates the type of changes observed in the fingerprint region of the Raman spectra of PPTA fibre upon exposure to D_2O. These results may not only be correlated with the fraction of amide sites on the surface of crystallites, but give insight into the structural origin of the accessibility of these materials which facilitates biological degradation[50].

DISCUSSION

PPTA as-polymerized polymer

Analysis of the X-ray diffraction data for as-polymerized PPTA finds that the crystallite dimensions in the direction perpendicular to the chain axis are ~3.0–3.5 nm and the cross-sectional shape is approximately circular. For crystallites of this size, ~40% of all chains reside on a surface. About one-half of the amide sites in chains located on a crystallite surface can hydrogen bond, hence the percentage of amide sites in the entire crystallite that cannot hydrogen bond must be 20% or greater. This finding may be compared to the observation in the n.m.r. experiments that 25% of the N-H sites are mobile at all accessible temperatures. These observations indicate that to first order the dynamic structure of the amide sites in as-polymerized PPTA polymer must consist of two populations: one associated with non-hydrogen-bonded mobile amide sites on the surface of crystallites and the other with immobile hydrogen-bonded sites located both on the surface of crystallites and predominantly in the crystallite interior. Furthermore, the identification of two types of sites with different dynamic properties is supported by the n.m.r. spin-lattice relaxation data for the terephthalamide rings and the *p*-phenylenediamine rings[31] which finds that the relaxation data may be partitioned, once again, into two components below 75°C with the faster relaxing component comprising 25%. (N.m.r. differentiation of polymer segments located on and within a crystal has been proposed previously for cellulose[51,52].)

Further insight into the heterogeneity of the dynamic structure can be obtained by examination of the ^2H n.m.r. lineshape data for the terephthalamide rings[30] and *p*-phenylene diamine rings[31]. These data indicate that there is a broad distribution of correlation times for the flipping rate of the *p*-phenylene diamine rings and an even broader or bimodal distribution of correlation times for the terephthalamide rings. These observations indicate that in addition to the first order dynamic structure description described above, each population must contain a variety of dynamical environments which reflect the heterogeneity of the dynamic structure within each population. It appears that the heterogeneity of the dynamic structure reflects not only the quite small dimensions of the crystallites perpendicular to the chain axis, but also the concomitant proximity of all chains to a crystallite surface and hence a substantial probability of structural imperfection throughout the crystallite. Further refinement of this model would involve constructing a more complete description of the degree of crystalline perfection from the X-ray diffraction data, but the absence of multiple orders in the diffraction pattern precludes this approach.

This microscopic model of one feature of the morphology of as-polymerized PPTA can be compared to the macroscopic accessibility of amide N-H bonds to water. In the D_2O exchange experiments, it was found that 30–40% of the amide N-H sites exchanged under very mild conditions. This indicates that not only are the non-hydrogen-bonded N-H sites on the crystallite surfaces accessible, but also another 10–20% of all sites are also accessible. This reflects, once again, not only the small dimensions of the crystallites, but also the lack of structural packing perfection which is necessary to permit accessibility.

PPTA fibre

The process of fibre formation results in increased structural perfection as evidenced by the substantial

change in crystallite dimensions perpendicular to the chain axis when comparing as-polymerized polymer (3.5 nm) to Kevlar® 29 (5.2 nm). More robust fibre processing results in even larger mean crystallite sizes in the plane perpendicular to the chain axis for Kevlar® 49 (7.2 nm × 6.0 nm) and Kevlar® 149 (13.3 nm × 8.7 nm). Concomitant with the increase in lateral crystallite size the accessibility to water decreases to ~25% for Kevlar® 29 and 49 and to ~10% for Kevlar® 149. These observations indicate that the fibre formation process can lead to an increased perfection of the structure as manifested both in increased lateral crystallite dimensions as well as decreased accessibility to water.

CONCLUSIONS

The description of the heterogeneous dynamic structure of as-polymerized PPTA and the limited description of the effect of fibre formation on this structure presented here allows us to more fully describe the morphology of these materials when taken in conjunction with the large number of studies extant in the literature. Our description focuses primarily on the effect of lateral crystallite dimensions on the microscopic dynamic structure and the concomitant macroscopic accessibility properties. This description is complementary to the supramolecular pleated sheet fibre structure previously described[14]. (The transition region between pleated sheets is too small a fraction of the total number of sites to account for the two populations observed in the n.m.r. results.) The idealized pleated sheet model can be extended to incorporate the small lateral crystallite dimensions described here. (Dobb *et al.*[14] explicitly note that their model is an idealized one and that additional details including the effect of skin–core morphology must be included for a more complete description.)

Furthermore, the conclusion that the heterogeneous dynamic structure reflects the imperfect structural consolidation of PPTA polymer and fibres is further supported by the observation of an equatorial streak in SAXS experiments; this result may be interpreted to indicate the presence of voids[53–56] or alternatively to reflect the presence of two types of crystal surfaces that either occur rather infrequently or the electron density difference between them is small (or both)[44]. Additionally, recent experimental and theoretical results[57] for the structure of rigid rod polymers indicate that polymer microfibrils may be composed of a number of smaller crystallites that meet at low energy lateral chain invariant interfaces to form a structure quite similar to that which we have found experimentally. The microcrystalline structure, formed by the imperfect structural consolidation that occurs during processing, is not only the origin of macroscopic accessibility for small molecules, but also provides a plausible structural basis for biological accessibility. Recent results[50] regarding the short lifetime of aramid fibrils in rat lungs indicate that the fibrils must be accessible *in vivo* so as to allow for their degradation.

ACKNOWLEDGEMENTS

The authors are indebted to Professor H. Chanzy for many insightful comments and suggestions as well as extensive consultations related to the microscopy. Additionally we would like to acknowledge P. A. Cooper, J. E. Frieda, M. J. VanKavelaar, and C. R. Walther for skilled technical assistance.

REFERENCES

1 Erman, B., Flory, P. J. and Hummel, J. P. *Macromolecules* 1980, **13**, 484
2 Yang, H. H. 'Aromatic High-Strength Fibers', SPE Monographs, Wiley-Interscience, New York, 1989
3 Tanner, D., Fitzgerald, J. A. and Phillips, B. R. *Adv. Mater.* 1989, **5**, 151
4 Roche, E. J., Allen, S. R., Gabara, V. and Cox, B. *Polymer* 1989, **30**, 1776
5 Haraguchi, K., Kajiyama, T. and Takayanagi, M. *J. Appl. Polym. Sci.* 1979, **23**, 915
6 Panar, M., Avakian, P., Blume, R. C., Gardner, K. H., Gierke, T. D. and Yang, H. H. *J. Polym. Sci., Polym. Phys. Edn* 1983, **21**, 1955
7 Northolt, M. G. *Eur. Polym. J.* 1974, **10**, 799
8 Northolt, M. G. and van Aertsen, J. J. *Polym. Lett. Edn* 1973, **11**, 333
9 Tashiro, K., Kobayashi, M. and Tadokoro, H. *Macromolecules* 1977, **10**, 413
10 Ii, T., Tashiro, K., Kobayashi, M. and Tadokoro, H. *Macromolecules* 1987, **20**, 347
11 Ii, T., Tashiro, K., Kobayashi, M. and Tadokoro, H. *Macromolecules* 1986, **19**, 1772
12 Barton, R. *J. Macromol. Sci. Phys.* 1986, **24**, 119
13 Ballou, J. W. *Am. Chem. Soc. Div. Polym. Chem., Polym. Prepr.* 1976, **17**, 75
14 Dobb, M. G., Johnson, D. J. and Saville, B. P. *J. Polym. Sci., Polym. Phys. Edn* 1977, **15**, 2201
15 Dobb, M. G., Johnson, D. J. and Saville, B. P. *J. Polym. Sci., Polym. Symp.* 1977, **58**, 237
16 Hagege, R., Jarrin, M. and Sotton, M. *J. Microscopy* 1979, **115**, 65
17 Shen, D. Y., Molis, S. E. and Hsu, S. L. *Polym. Eng. Sci.* 1983, **23**, 543
18 Chatzi, E. G., Urban, M. W., Ishida, H. and Koenig, J. L. *Polymer* 1986, **27**, 1850
19 Penn, L. and Milanovich, F. *Polymer* 1979, **20**, 31
20 Prasad, K. and Grubb, D. T. *J. Appl. Polym. Sci.* 1990, **41**, 2189
21 Woodward, A. D., Landis, J. and Frosini, V. *J. Polym. Sci., Polym. Phys. Edn* 1972, **10**, 2051
22 Sugiya, I., Kobayashi, S., Iwayanagi, S. and Shibata, T. *Polym. J.* 1982, **14**, 43
23 English, A. D. *J. Polym. Sci., Polym. Phys. Edn* 1986, **24**, 805
24 Hong, J. and Harbison, G. S. *Am. Chem. Soc. Div. Polym. Chem., Polym. Prepr.* 1990, **31**, 115
25 Fukuda, M., Kawai, H., Horii, F. and Kitamaru, R. *Polym. Commun.* 1988, **29**, 97
26 Cain, E. J., Gardner, K. H., Gabara, V., Allen, S. R. and English, A. D. *Am. Chem. Soc. Div. Polym. Chem., Polym. Prepr.* 1990, **31**, 518
27 Cain, E. J., Gardner, K. H., Gabara, V., Allen, S. R. and English, A. D. *Macromolecules* 1991, **24**, 3721
28 Schadt, R. J., Cain, E. J., Gardner, K. H., Gabara, V., Allen, S. R. and English, A. D. *Am. Chem. Soc. Div. Polym. Chem., Polym. Prepr.* 1991, **32**, 253
29 English, A. D., Gardner, K. H., Schadt, R. J., Cain, E. J., Gabara, V. and Allen, S. R. *Am. Chem. Soc. Div. Polym. Chem., Polym. Prepr.* 1992, **33**, 82
30 Schadt, R. J., Cain, E. J., Gardner, K. H., Gabara, V., Allen, S. R. and English, A. D. *Macromolecules* 1993, **26**, 6503
31 Schadt, R. J., Gardner, K. H., Gabara, V., Allen, S. R., Chase, D. B. and English, A. D. *Macromolecules* 1993, **26**, 6509
32 Li, Y., Wu, C. and Chu, B. *J. Polym. Sci., Polym. Phys. Edn* 1991, **29**, 1309
33 Chu, B., Wu, C., Li, Y., Harbison, G. S., Roche, E. J., Allen, S. R., McNulty, T. F. and Phillips, J. C. *J. Polym. Sci., Polym. Lett. Edn* 1990, **28**, 227
34 Shubha, M., Parimala, V. and Vijayan, K. *J. Mater. Sci. Lett.* 1991, **10**, 1377
35 Allen, S. R. and Roche, E. J. *Polymer* 1989, **30**, 996
36 Allen, S. R., Roche, E. J., Bennett, B. and Molaison, R. *Polymer* 1992, **33**, 1849
37 Nakamae, K., Nishino, T. and Airu, X. *Polymer* 1992, **33**, 4898
38 Weinkauf, D. H., Kim, H. D. and Paul, D. R. *Macromolecules* 1992, **25**, 788

39 Fukuda, M., Ochi, M., Miyagawa, M. and Kawai, H. *Textile Res. J.* 1991, **61**, 668
40 Wang, J. Z., Dillard, D. A. and Ward, T. C. *J. Polym. Sci., Polym. Phys. Edn* 1992, **30**, 1391
41 Le, C. V. and Ly, N. G. *Textile Res. J.* 1993, **63**, 57
42 Hirschinger, J., Miura, H., Gardner, K. H. and English, A. D. *Macromolecules* 1990, **23**, 2153
43 Chapman, G. E., Campbell, I. D. and McLaughlan, K. A. *Nature* 1970, **225**, 639
44 Grubb, D. T., Prasad, K. and Adams, W. *Polymer* 1991, **32**, 1167
45 Sherman, E. S., Adams, W. W. and Thomas, E. L. *J. Mater. Sci.* 1981, **16**, 1
46 Riewald, P. G., Dhingra, A. and Chern, T. S. in 'Sixth International Conference on Composite Materials', Elsevier, New York, 1987, p. 362
47 Schadt, R. J. and English, A. D. *J. Phys. Chem.* 1993, **97**, 8387
48 Heaton, N. J., Vold, R. L. and Vold, R. R. *J. Am. Chem. Soc.* 1989, **111**, 3211
49 Heaton, N. J., Vold, R. R. and Vold, R. L. *J. Chem. Phys.* 1989, **91**, 56
50 Warheit, D. B., Kellar, K. A. and Hartsky, M. A. *Toxicol. Appl. Pharmacol.* 1992, **116**, 225
51 Atalla, R. H. and VanderHart, D. L. *Science* 1984, **223**, 283
52 Sugiyama, J., Vuong, R. and Chanzy, H. *Macromolecules* 1991, **24**, 4168
53 Dobb, M. G., Johnson, D. J., Majeed, A. and Saville, B. P. *Polymer* 1979, **20**, 1284
54 Hindeleh, A. M., Hosemann, R., Hinrichsen, G. and Springer, H. *Polym. Commun.* 1990, **31**, 205
55 Hindeleh, A. M. and Abdo, M. *Polymer* 1989, **30**, 218
56 Aerts, J. *J. Appl. Cryst.* 1991, **24**, 709
57 Martin, D. C. and Thomas, E. L. *Phil. Mag. A* 1991, **64**, 903